Buffer-gas-induced absorption resonances in Rb vapor

Eugeniy E. Mikhailov,* Irina Novikova, Yuri V. Rostovtsev, and George R. Welch
Department of Physics and Institute for Quantum Studies, Texas A&M University, College Station, Texas 77843-4242, USA
(Received 23 September 2003; revised manuscript received 8 June 2004; published 20 September 2004)

We observe transformation of the electromagnetically induced transparency (EIT) resonance into an absorption resonance in a Λ interaction configuration in a cell filled with ^{87}Rb and a buffer gas. This transformation occurs as one-photon detuning of the coupling fields is varied from the atomic transition. No such absorption resonance is found in the absence of a buffer gas. The width of the absorption resonance is several times smaller than the width of the EIT resonance, and the changes of absorption near these resonances are about the same. Similar absorption resonances are detected in the Hanle configuration in a buffered cell.

DOI: 10.1103/PhysRevA.70.033806 PACS number(s): 42.50.Gy

I. INTRODUCTION

The coherent interaction of atoms with electromagnetic fields has attracted increasing attention recently in studies of nonlinear and quantum optics as well as in spectroscopy and precision metrology. Under the combined action of several resonant laser fields, atoms are optically pumped into a coherent superposition of the ground state (hyperfine or magnetic) sublevels which is decoupled from the original electromagnetic fields. That is, the atoms are in a so-called "dark" state. Such a medium possesses some unique optical properties, for example, coherent population trapping (CPT) [1–3], cancellation of absorption due to electromagetically induced transparency (EIT) [4–6], and steep nonlinear dispersion [4,7–9]. The characteristic spectral width of features occurring due to these nonlinear effects is determined by the inverse lifetime of an atom in the coherent superposition of ground states. Since radiative transitions are usually forbidden between these states, the coherence can be preserved for a long time, and in atomic cells its lifetime is usually determined by the interaction time of the atom with the laser beams [10,11].

The addition of a buffer gas (inert gases, N_2, CO_2, CH_4, etc.) to the atomic vapor is a common method for obtaining narrow EIT resonances. Because of the extremely low spin-exchange cross section, the collisions between rubidium and buffer gas atoms or molecules do not destroy the quantum coherence of the internal states of the atoms, but effectively prolong the time they stay inside the laser beam(s). The processes of decoherence and redistribution of atomic population have been extensively studied in optical pumping experiments [12–14]. Substantial narrowing of the dark resonance linewidth is reported in [15–18].

In this paper we study the transformation of the transmission peaks corresponding to EIT into enhanced absorption peaks for proper laser detuning. We present an extensive experimental and theoretical analysis of this effect, previously reported in [19,20]. We observe narrow enhanced absorption resonances in two experimental arrangements: in a bichromatic configuration, where strong and weak laser fields form a Λ scheme on two ground-state hyperfine sublevels [Fig. 1(a)], and in the degenerate Hanle configuration [Fig. 1(b)]. In both situations EIT resonance is observed for the laser field(s) tuned to the atomic transition(s) due to formation of a noninteracting ground-state atomic coherence; in both cases the line shape of this transmission peak persists for any value of the one-photon detuning unless a buffer gas is added to the Rb vapor.

Before proceeding to the details of the experiment let us highlight the distinctions between the effect described below and similar looking coherent effects.

(i) Transformation of enhanced transmission to enhanced absorption CPT resonance has been reported by Affolderbach *et al.* [21] in their experiments with a bichromatic standing wave in hot atomic vapor. Because of large Doppler broadening, moving atoms effectively interact with a double-Λ-level configuration, which may result in either suppression or enhancement of absorption, depending on the relative phases of the driving fields. This explanation, however, cannot be applied to the present experimental data, since our experiments are carried out with running waves.

(ii) Narrow absorption resonances in alkali-metal vapors are also a manifestation of electromagnetically induced absorption (EIA) [22–28], or the closely related enhanced absorption Hanle effect [29–33]. In those experiments, a narrow absorption peak appears for two laser fields of close frequencies interacting with a quasidegenerate two-level system. However, it is a general requirement in both cases that the degeneracy of the ground state must be lower than that of the excited state, i.e., $F<F'$, which prohibits any dark state formation. Narrow EIA resonances in this case are due to spontaneous coherence transfer from the excited states of the atoms [25,26,34]. In addition, the experimental arrangements for traditional EIA experiments involve laser fields resonant with the corresponding atomic transitions, whereas the narrow absorption resonances discussed in this paper appear for far-detuned laser fields.

(iii) Finally, the effect described below cannot be attributed to pressure-induced extra resonance (PIER) (for a review of collision-induced coherent effects, see [35]). In PIER the extra resonance is connected to a dressed-state population that is nonvanishing only in the presence of collisions. The relatively low buffer gas pressure used in our experiment does not allow the realization of PEIR.

*Electronic address: evmik@leona.physics.tamu.edu

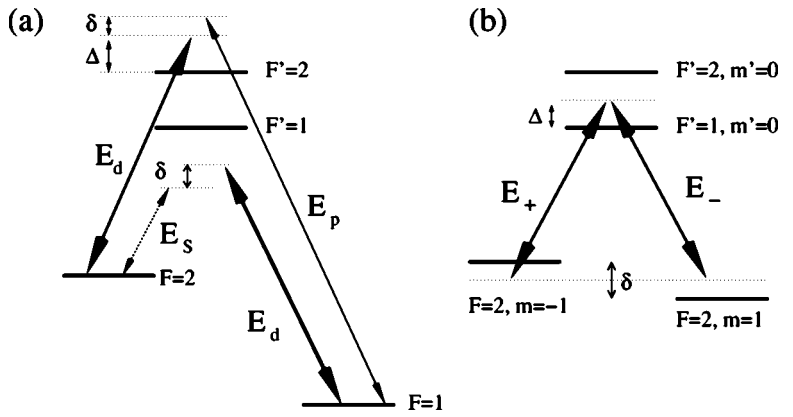

FIG. 1. (a) Three-level interaction scheme of three laser fields with ^{87}Rb atoms: the long-lived coherence is created on hyperfine ground-state sublevels with strong driving field E_d and weak probe (anti-Stokes) field E_p; the probe and Stokes fields E_s are generated by electro-optic modulation. (b) Hanle configuration: the ground-state coherence is created on magnetic sublevels with two circularly polarized components $E_\pm$ of a monochromatic linearly polarized laser field. In both cases Δ is the one-photon detuning of the laser(s) from atomic resonance, and δ is the two-photon detuning due to frequency mismatch in case (a) or an external magnetic field in case (b).

This paper is organized as follows. In the next section we describe the experimental apparatus and measurement technique. In Sec. III we present the experimental study of these resonances in a three-level Λ scheme based on hyperfine coherence in atomic cells with different amounts of a buffer gas. A theoretical analysis is given in Sec. IV. Resonant four-wave mixing and the line shape of the associated resonances in a Stokes field are discussed in Sec. V. A brief analysis of the coherent resonance widths is given in Sec. VI. In Sec. VII, we present the experimental results for the enhanced absorption resonances observed in the Hanle configuration, together with a qualitative discussion of their origin. A brief summary of the work appears in the final section.

II. EXPERIMENTAL SETUP

A schematic of the experimental setup is shown in Fig. 2. An external cavity diode laser is tuned to the $5S_{1/2} \rightarrow 5P_{1/2}$ (D_1) transition of ^{87}Rb. A probe field E_p (and an additional Stokes field E_S) are produced by an electro-optic modulator (EOM) driven by a stable narrowband tunable microwave generator operating at 6.835 GHz to match the ^{87}Rb ground-state hyperfine transition frequency. The probe and Stokes fields have equal intensities of approximately 10% of that of the drive field. After the EOM, all fields pass through a single-mode optical fiber to create a clean spatial mode with a Gaussian radial intensity distribution and to increase the diameter of the output beam to 7 mm. The fields are circularly polarized with a quarter-wave plate placed after the fiber.

In this experiment we use several glass cells filled with isotopically enhanced ^{87}Rb and various pressures and types (Ne, Kr) of buffer gas. Each cell is placed inside a three-layer magnetic shield to screen the laboratory magnetic field from the system and is heated to 60 °C to increase the density of the ^{87}Rb vapor to approximately 2.5×10^{11} cm^{-3}. After traversing the cell, all three fields are mixed on a fast photodiode with an additional field shifted by 60 MHz with respect to the driving field. The resulting photocurrent is measured with a spectrum analyzer to separate the transmission signals of the probe and Stokes components (see Fig. 2). This detection scheme has been described in [36,37].

For our studies in the Hanle configuration, the electro-optical modulator is removed so that there is only one linearly polarized monochromatic electromagnetic field propagating through the cell. The transmitted intensity is recorded directly from a photodetector. A longitudinal magnetic field for shifting the Zeeman sublevels is created by a solenoid mounted inside the inner magnetic shield.

III. ENHANCED ABSORPTION DUE TO A BUFFER GAS IN HYPERFINE Λ SCHEME

We start with the drive field resonant with the $5S_{1/2}F=2 \rightarrow 5P_{1/2}F'=2$ transition; simultaneously, the probe field couples the ground-state $5S_{1/2}F=1$ level to the same excited state. In that resonant Λ system we observe the expected narrow EIT resonance in the probe field transmission due to efficient optical pumping into a noninteracting dark state. The bottom row of Fig. 3 shows the observed resonances for cells with different amounts of buffer gas. It is easy to see that all EIT peaks are nearly symmetric, which is in agreement with theoretical predictions [38–41] and our numerical simulations. The main difference between different cells is the narrowing of the EIT width resulting from the increased interaction time for higher buffer gas pressure.

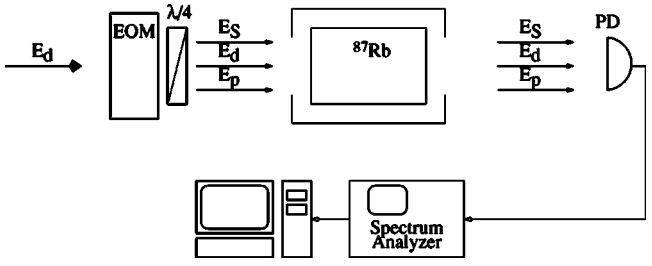

FIG. 2. Schematic of the experimental setup.

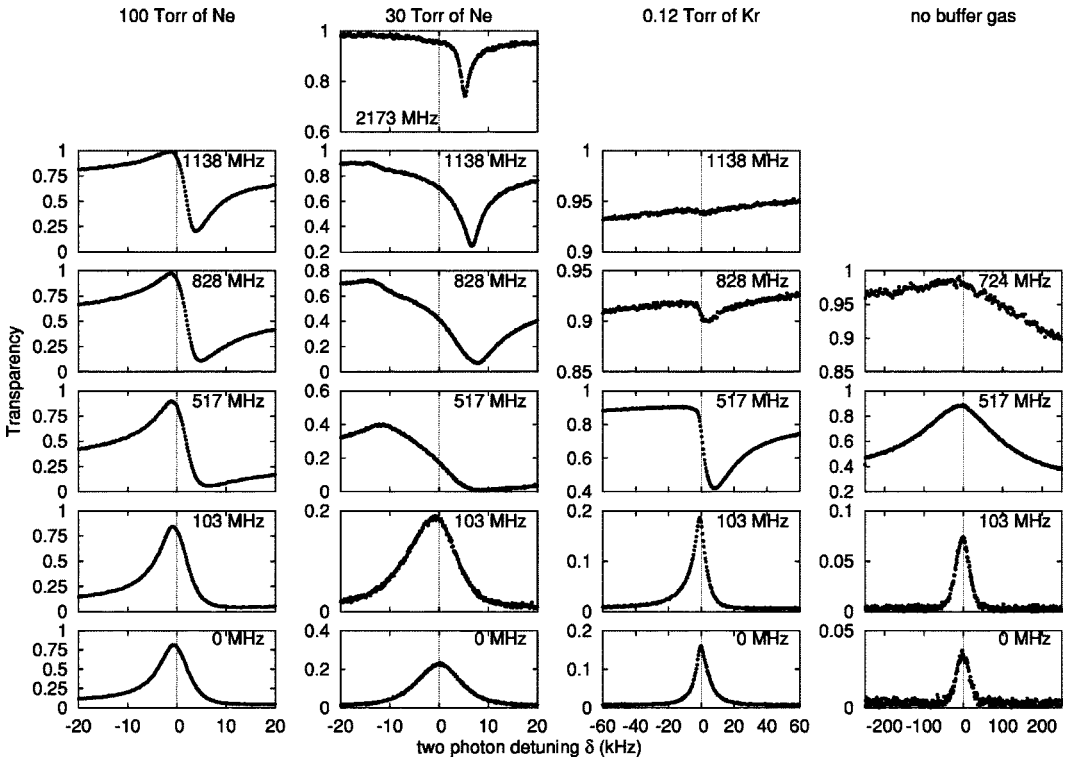

FIG. 3. Transmission of the probe field as a function of two-photon detuning δ for various one-photon detunings Δ. The values of Δ are shown on the upper right corner of each graph. These data are recorded in the presence of (columns, left to right) 100 Torr of Ne, 30 Torr of Ne, 0.12 Torr of Kr, and no buffer gas. All signals are normalized to the nonabsorbed transmission. The asymmetry of the resonance curves for $\Delta=828$ and 1138 MHz in the cell with 0.12 Torr Kr and for $\Delta=517$ and 724 MHz in the vacuum cell is due to the slope of the one-photon absorption contour. The intensities of the laser fields are $I_d \simeq 1.20$ mW/cm^2 and $I_p \simeq 0.13$ mW/cm^2.

As we tune the laser away from the atomic transition (while maintaining near-zero two-photon detuning) the shape of the transmission resonance changes depending on the presence of a buffer gas in a cell. For the vacuum cell (the rightmost column in Fig. 3) the resonance stays symmetric while its width increases rapidly with one-photon detuning Δ due to the less efficient density narrowing.

However, the behavior is very different in cells with a buffer gas. As Δ increases, the EIT resonance becomes asymmetric, and then gradually transforms into a narrow *absorption* resonance. Let us emphasize here some of the important properties of these resonances. For example, the cell with 30 Torr of Ne (Fig. 3) shows that the amplitude of the enhanced absorption peak observed for large detuning ($\Delta \approx 1-2$ GHz) is comparable to, and sometimes larger than, the amplitude of the EIT peak at $\Delta=0$, and its width is narrower. Second, these narrow absorption resonances are observed for the laser detuning exceeding the Doppler-broadened one-photon resonant absorption width ($\Delta>1$ GHz). Thus, the enhanced absorption peaks appears on top of 100% transmission of the probe field.

The asymmetry in the EIT resonances for nonzero one-photon detuning of the laser fields has been observed by Levi *et al.* [42] in maser emission in the CPT process as well as by Knappe *et al.* [43]. However, the reported modification of the resonance line shape is significantly weaker. Knappe *et al.* also suggested an empirical expression for the resonance line shape:

$$f(\delta) = \tilde{\gamma}\frac{A\tilde{\gamma} + B(\delta - \delta_0)}{\tilde{\gamma}^2 + (\delta - \delta_0)^2} + C. \tag{1}$$

Here δ is the two-photon (Raman) detuning, $\tilde{\gamma}$ is the effective width of the coherent resonance, and A, B, and C are fitting parameters which are functions of the one-photon detuning Δ. We introduce a shift δ_0 of the resonance position from the exact Raman condition to reproduce the experimental data. One can see that this expression consists of symmetric and antisymmetric Lorentzian functions of δ with amplitudes A and B, respectively. The parameter C reflects the residual absorption of the electromagnetic field determined by incoherent processes. Taichenachev *et al.* [44] derived the analytical expressions for these coefficients in the limit of weak interaction fields (perturbation approach). The case of a strong (drive) field is discussed in the next section.

It is convenient to write the coefficients A and B in the following form:

$$A = D\cos(\phi), \quad B = D\sin(\phi), \tag{2}$$

so that Eq. (1) can be written as

$$f(\delta) = \mathrm{Re}\left\{ D(\Delta)e^{i\phi(\Delta)}\frac{\tilde{\gamma}}{\tilde{\gamma} + i(\delta - \delta_0)} \right\} + C. \tag{3}$$

In this case, the parameter D characterizes the amplitude of the resonance, and the angle ϕ expresses the ratio between the symmetric and antisymmetric components in Eq. (1). For

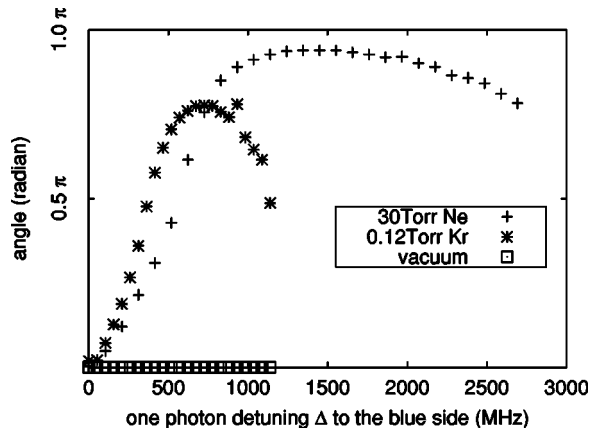

FIG. 4. Angle ϕ of two-photon resonance for ^{87}Rb cells with different amounts of a buffer gas.

example, $\phi=0$ represents a symmetric peak of enhanced transmission, $\phi=\pi$ corresponds to a symmetric peak of enhanced absorption, and $\phi=\pm\pi/2$ corresponds to a pure dispersion-like line shape.

These parameters are shown as functions of one-photon detuning in different cells in Figs. 4 and 5. We note that no deviation from the symmetric Lorentzian form is observed for the EIT resonance in a vacuum cell ($\phi=0$ for all detunings). However, buffered cells show the change from a symmetric transmission resonance (for $\Delta=0$) to an almost symmetric absorption resonance for $\Delta\approx 700$ MHz for 0.12 Torr buffer gas pressure and $\Delta\approx 1.4$ GHz for 30 Torr buffer gas pressure. After reaching its maximum, the angle starts to decline again, although we never observe the recovery of the symmetric EIT peak for larger detunings.

IV. THEORETICAL ANALYSIS

Let us first give a brief pictorial explanation of the effect. The observation of the narrow absorption resonance for large laser detunings may be qualitatively understood by using the dressed-state picture. It is known that the interaction of the drive field with the transition between levels $|a\rangle$ and $|c\rangle$ can

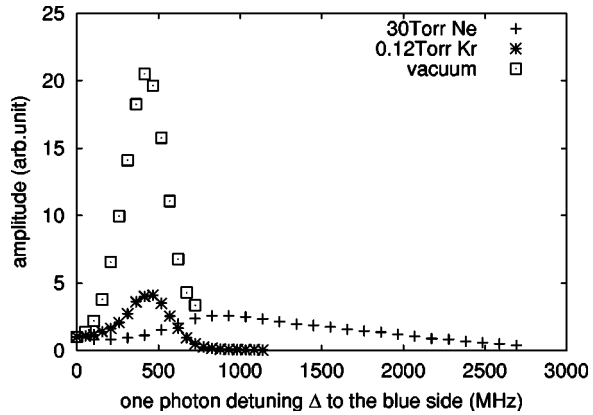

FIG. 5. Amplitude D of the two-photon resonance. For easier comparison, the values of D are normalized to the resonance amplitude at zero detuning.

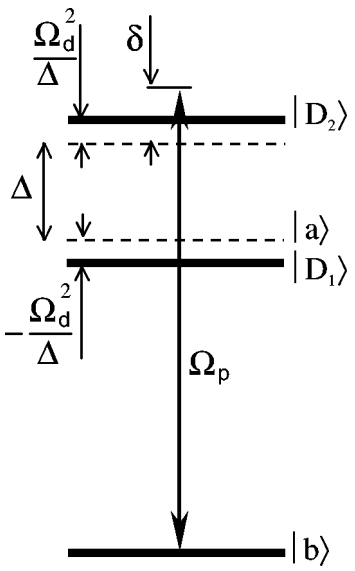

FIG. 6. Dressed-states picture for three-level Λ scheme. State $|D_1\rangle=\xi_1[|a\rangle+(\Omega_d/\Delta)|c\rangle]$ has approximately the same energy as bare state $|a\rangle$, and state $|D_2\rangle=\xi_2[|c\rangle-(\Omega_d^*/\Delta)|a\rangle]$ is close to the two-photon resonance. The normalization coefficients are $\xi_{1,2}\approx 1+o(|\Omega_d|^2/\Delta^2)$. EIT is observed for $\delta=0$ (maximum quantum interference), and absorption resonance corresponds to $\delta=-|\Omega_d|^2/\Delta$ (probe is resonant with $|D_2\rangle$).

be described as a splitting of the excited state [45]. Figure 6 shows the interaction scheme for the probe beam in the case of the far-detuned drive field ($\Delta\gg|\Omega_d|,\gamma_r$).

For these conditions the transition between one of the dressed states ($|D_1\rangle$ in our notation) and level $|b\rangle$ corresponds to a regular resonant absorption, and the transition between another dressed state $|D_2\rangle$ and level $|b\rangle$ corresponds to a two-photon Raman transition. The destructive interference of the two dressed states occurs only in the case of zero two-photon detuning between probe and drive fields and corresponds to the frequency with zero absorption (EIT). For the ideal case of $\gamma_{bc}=0$ (no ground-state relaxation) and assuming that all population is in level $|b\rangle$, the magnitudes of absorption and Raman transition are the same while their widths are different: the width of the former is determined by the relaxation rate of optical coherence γ, while the width of the Raman transition is given by $\gamma|\Omega_d|^2/\Delta^2$ and can be small for large Δ. However, if spin relaxation is not zero, the amplitude of the resonance dramatically decreases once the absorption resonance is narrower than this relaxation, and for $\gamma_{bc}\gg\gamma|\Omega_d|^2/\Delta^2$ the line disappears. The addition of a buffer gas, therefore, improves the conditions for the observation of that narrow resonance: higher buffer gas pressure produces additional pressure broadening of the excited state (i.e., makes γ bigger) and at the same time restricts the diffusion of Rb atoms through the interaction region (i.e., makes γ_{bc} smaller).[1]

The dressed state picture provides a general idea about origin of the narrow absorption resonances. Note, that the

[1]Recently the subnatural narrowing of the Doppler-free resonance for far-detuned incoherent fields in a vacuum cell has been demonstrated by Rapol *et al.* [73].

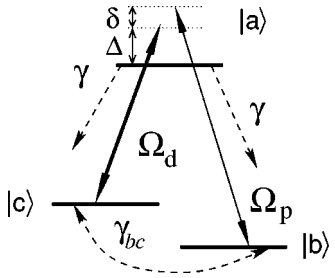

FIG. 7. Three-level Λ system.

asymmetric lineshapes observed in the experiment cannot be fitted by the combination of two symmetric Lorentzian peaks—one positive due to coherent population trapping in the dark state and one negative due to the enhanced absorption by the bright state. The interference between two dressed state has to be taken into account for proper description of the coherent effects [46].

For more rigorous analysis we derive an expression for the absorption coefficient of a weak probe field in Rb atoms. It has been shown that a closed three-level Λ scheme as shown in Fig. 7 provides a satisfactory description of coherent effects in alkali-metal atoms [41]. The propagation equations for the density matrix elements are well known (see, e.g., [41]) and are the following:

$$\dot{\rho}_{bb} = i\Omega_p^*\rho_{ab} - i\Omega_p\rho_{ba} + \gamma_r\rho_{aa} - \gamma_{bc}\rho_{bb} + \gamma_{bc}\rho_{cc}, \tag{4}$$

$$\dot{\rho}_{cc} = i\Omega_d^*\rho_{ac} - i\Omega_d\rho_{ca} + \gamma_r\rho_{aa} - \gamma_{bc}\rho_{cc} + \gamma_{bc}\rho_{bb}, \tag{5}$$

$$\dot{\rho}_{ab} = -\Gamma_{ab}\rho_{ab} + i\Omega_p(\rho_{bb} - \rho_{aa}) + i\Omega_d\rho_{cb}, \tag{6}$$

$$\dot{\rho}_{ca} = -\Gamma_{ca}\rho_{ca} + i\Omega_d^*(\rho_{aa} - \rho_{cc}) - i\Omega_p^*\rho_{cb}, \tag{7}$$

$$\dot{\rho}_{cb} = -\Gamma_{cb}\rho_{cb} - i\Omega_p\rho_{ca} + i\Omega_d^*\rho_{ab}, \tag{8}$$

where $\Omega_d = \wp_{ac}E_p/\hbar$ and $\Omega_p = \wp_{ab}E_d/\hbar$ are the Rabi frequencies of the drive and probe fields. The generalized decay rates are defined as

$$\Gamma_{ba} = \gamma + i(\Delta + \delta), \tag{9}$$

$$\Gamma_{ca} = \gamma + i\Delta, \tag{10}$$

$$\Gamma_{bc} = \gamma_{bc} + i\delta. \tag{11}$$

Here $\gamma = \gamma_r + \gamma_{\mathrm{deph}}$ is the polarization decay rate, $\gamma_r \simeq 2\pi \times 3$ MHz is the radiative decay rate of the excited state, γ_{deph} is the dephasing rate of the optical transition due to nonradiative effects ($\gamma_{\mathrm{deph}}/p \simeq 5$ MHz/Torr [47]); γ_{bc} is the inverse lifetime of the coherence between ground states $|b\rangle$ and $|c\rangle$, which is determined by the diffusion time of Rb atoms through the interaction region and the nonhomogeneity of the magnetic field due to imperfect screening. The presence of the buffer gas affects the values of both γ_{bc} and γ. On one hand, it allows for a longer ground-state coherence lifetime. On the other hand it broadens the optical transition, since γ_{deph} grows linearly with buffer gas pressure [48].

Solving Eqs. (4)–(8) in the steady state regime and assuming $|\Omega_p| \ll |\Omega_d|$, we obtain the following expression for the linear susceptibility of the probe field:

$$\chi = i\kappa\frac{\Gamma_{cb}(\rho_{aa}^{(0)} - \rho_{bb}^{(0)}) + (|\Omega_d|^2/\Gamma_{ca})(\rho_{aa}^{(0)} - \rho_{cc}^{(0)})}{\Gamma_{ab}\Gamma_{cb} + |\Omega_d|^2}, \tag{12}$$

where $\kappa = (3/8\pi)N\lambda^2\gamma_r$, N is the ^{87}Rb density, and λ is the wavelength of the probe field.

The atomic population differences in the approximation of strong driving field ($|\Omega_d|^2 \gg \gamma_{bc}\gamma$) are

$$(\rho_{aa}^{(0)} - \rho_{bb}^{(0)}) \simeq -\frac{\gamma_{bc}\Delta^2 + \gamma|\Omega_d|^2}{2\gamma_{bc}\Delta^2 + \gamma|\Omega_d|^2}, \tag{13}$$

$$(\rho_{aa}^{(0)} - \rho_{cc}^{(0)}) \simeq -\frac{\gamma_{bc}(\Delta^2 + \gamma^2)}{2\gamma_{bc}\Delta^2 + \gamma|\Omega_d|^2}. \tag{14}$$

By substituting these expressions into Eq. (12), we find the absorption coefficient $\alpha = \mathrm{Im}\{\kappa\}$ as a function of the two-photon detuning δ:

$$\alpha = \frac{\kappa}{\gamma^2 + \Delta^2}\frac{\gamma_{bc}\Delta^2 + \gamma|\Omega_d|^2}{2\gamma_{bc}\Delta^2 + \gamma|\Omega_d|^2}\frac{\gamma_{bc}|\Omega_d|^2 + \gamma\delta^2}{\tilde{\gamma}^2 + (\delta - \delta_0)^2}, \tag{15}$$

where

$$\delta_0 = |\Omega_d|^2\frac{\Delta}{\gamma^2 + \Delta^2} \tag{16}$$

is the ac Stark shift of the excited state, and

$$\tilde{\gamma} = \frac{\sqrt{\gamma^2|\Omega_d|^4 + \gamma_{bc}^2\Delta^2(\gamma^2 + \Delta^2)}}{\gamma^2 + \Delta^2} \tag{17}$$

is the effective width of the two-photon transmission resonance.

Using Eq. (15) for the absorption coefficient we can now find expressions for the coefficients A, B, and C in Eq. (1) which describe the line shape of the two-photon resonance for the probe field propagating through a medium of length L. For the moment we restrict ourselves to the case of optically thin media, so that $I_p(z) = I_p(0)e^{-\alpha z} \simeq I_p(0)(1 - \alpha z)$:

$$A = \kappa L\,\eta\frac{|\Omega_d|^2}{\gamma^2 + \Delta^2}\frac{\gamma|\Omega_d|^2(\gamma^2 - \Delta^2) - \gamma_{bc}(\gamma^2 + \Delta^2)^2}{\gamma^2|\Omega_d|^4 + \gamma_{bc}^2\Delta^2(\gamma^2 + \Delta^2)}, \tag{18}$$

$$B = -\kappa L\,\eta\frac{\Delta}{\gamma^2 + \Delta^2}, \tag{19}$$

$$C = 1 - \kappa L\,\eta\frac{\gamma}{\gamma^2 + \Delta^2}, \tag{20}$$

$$\eta = \frac{\gamma_{bc}\Delta^2 + \gamma|\Omega_d|^2}{2\gamma_{bc}\Delta^2 + \gamma|\Omega_d|^2}. \tag{21}$$

It is easy to see that the coefficient C is well approximated by the absorption of a weak probe field in a two-level scheme. The only difference is the coefficient η, which describes the redistribution of the atomic population between

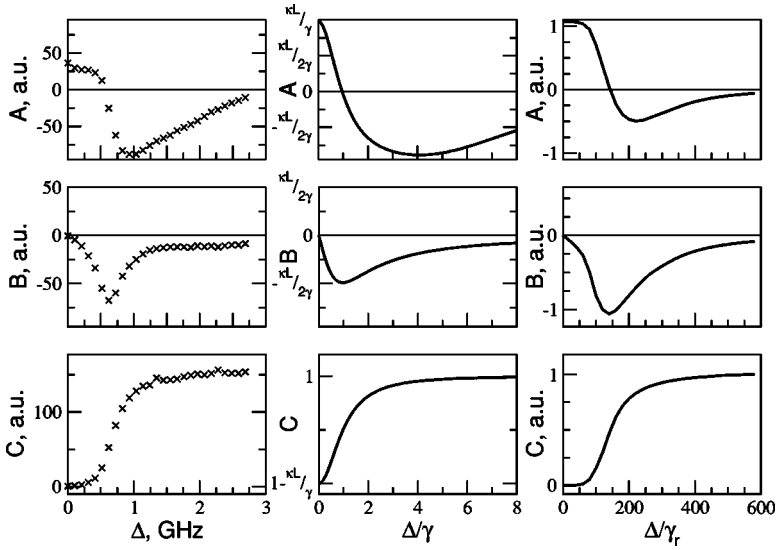

FIG. 8. Coefficients *A*, *B*, and *C* describing the line shape of the coherent resonance Eq. (1): extracted from the experimental data for ^{87}Rb cell with 30 Torr (left column), calculated using Eqs. (18)–(20) (middle column), and obtained by numerical modeling (right column).

ground levels due to optical pumping: in the case of a small one-photon detuning ($\Delta \ll |\Omega_d|\sqrt{\gamma/\gamma_{bc}}$) almost all atoms are in the state $|b\rangle$ and therefore $\eta=1$, and if the laser is far detuned, the populations of the levels $|b\rangle$ and $|c\rangle$ are almost the same and $\eta=1/2$.

The coefficient *A*, which describes the symmetric component of the resonant line shape, is a symmetric function of the one-photon detuning. Its sign changes as Δ gets larger: *A* is positive for small detunings, then it becomes negative at $\Delta \approx \gamma - 2\gamma_{bc}\gamma^2/|\Omega_d|^2$ (i.e., the resonance becomes absorptive). The coefficient *B* is an odd function of Δ, and exactly zero for $\Delta=0$.

A comparison of coefficients *A*, *B*, and *C* given by Eqs. (18)–(20) with those obtained by fitting our experimental data for the Rb cell with 30 Torr of Ne is presented in Fig. 8. One can immediately see that the theoretical formulas qualitatively describe the dependence of the coefficients as functions of one-photon detuning, although they are not accurate enough for a quantitative analysis. There are several reasons for this. On one hand, we will show below that the thermal velocity distribution of Rb atoms is very important and has to be taken into account. On the other hand, we assumed for simplicity that the medium is optically thin, which is not the case. One of the consequences of using an optically thick medium is density narrowing of the EIT resonances, which will be discussed in the following section.

We perform a numerical simulation of the interaction of the drive and probe fields with the three-level Λ system considered above. Our model takes into account attenuation of both drive and probe fields as they propagate through Rb vapor. The thermal motion of the atoms also implies that atoms with different velocities "see" the electromagnetic fields at shifted frequencies, and the final susceptibility has to be averaged over the Maxwell velocity distribution:

$$\chi(\Delta) = \frac{1}{\sqrt{\pi}ku}\int_{-\infty}^{+\infty} \chi(\Delta - kv)e^{-(kv)^2/(ku)^2}d(kv), \qquad (22)$$

where $k=\nu_d/c$ is the drive field wave vector, and $u=\sqrt{2k_BT/M}$ is the most probable thermal speed (here *T* is the temperature of the vapor, *M* is the mass of the Rb atom, and k_B is the Boltzmann constant). The residual Doppler broadening of the ground-state transition (Δku) may be neglected due to the Lamb-Dicke effect [18].

We can reproduce experimental spectra very accurately (compare the experimental spectra presented in Fig. 3 with the the results of numerical simulations in Fig. 9) except for the case of cells with small amounts of a buffer gas (<1 Torr). This limit corresponds to the regime where the mean free path of Rb atoms is comparable with the size of the interaction region. Under these conditions the motion of Rb atoms in and out of the laser beam has to be taken into account when calculating the ground-state coherence lifetime. Unfortunately, this mechanism is beyond the theoretical model used in our numeric simulations. For that reason we do not show any calculated transmission spectra for the cell with 0.12 Torr of Kr. The results of the numerical simulation for the parameters *A*, *B*, and *C* are shown in Fig. 8(c).

The calculated values of the resonance amplitude *D* and the ratio ϕ are shown in Figs. 10 and 11. These demonstrate that the inversion of the EIT resonance occurs in the cell with a buffer gas, whereas no absorption resonances ever appear in the cell without a buffer gas. Although a noticeable asymmetry of the resonance is expected for large laser detuning ($\Delta > 100\gamma_r$), the amplitude of the resonances is very small and hardly detectable.

It is also easy to see in Fig. 3 that for nonzero detuning Δ the centers of both EIT and buffer-gas-induced absorption resonances are shifted from zero two-photon detuning. One of the reasons for this effect is light shifts of the atomic levels, as shown by Eq. (16). However, this expression fails to describe the behavior of the resonance shift measured experimentally (Fig. 12). A more realistic resonance shift as a function of laser detuning is obtained by numerical simulation if Doppler averaging is performed (Fig. 12, inset).

We note that both the prediction of the theoretical model and the result of the numerical simulations provide only qualitative agreement with the experimental results. There are several major effects which are not considered here. For example, neither the hyperfine structure of the excited state

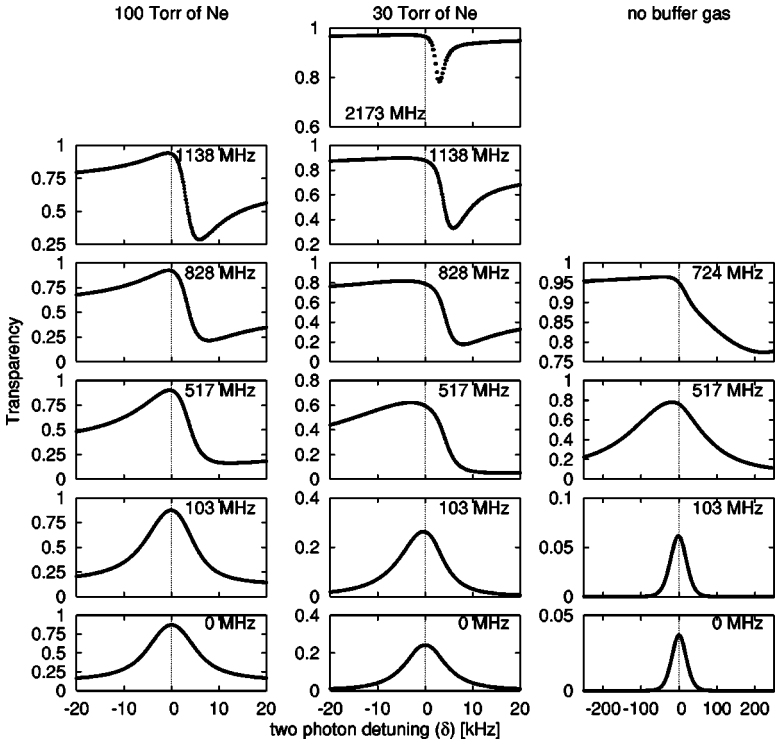

FIG. 9. Calculated probe field transmission spectra for the conditions corresponding to the experimental data in Fig. 3. We use the following parameters: $\gamma_{\mathrm{deph}}=450$ MHz, $\gamma_{bc}=0.5$ kHz for the cell with 100 Torr of Ne; $\gamma_{\mathrm{deph}}=150$ MHz, $\gamma_{bc}=0.7$ kHz for the cell with 30 Torr of Ne; and $\gamma_{\mathrm{deph}}=0$, $\gamma_{bc}=30$ kHz for the cell without a buffer gas. These values are in good agreement with published results for collisional dephasing [47,49]. For all graphs $ku=250$ MHz, $\Omega_d=2.5$ MHz, and $\Omega_p=0.5$ MHz. These values are reasonably close to the estimated actual Rabi frequencies $\Omega_d=2.1$ MHz and $\Omega_p=0.7$ MHz. The small deviation between them can be attributed to the nonuniform spatial distribution of the laser intensities.

nor the Zeeman substructure of all states is taken into consideration, although this may have a profound effect on the coherent interaction. In addition, no influence of the four-wave mixing processes is taken into account.

For better understanding of the conditions for which the enhanced absorption resonance occurs, we numerically compare the resonance line shape at a large one-photon detuning ($\Delta=250\gamma_r$) for the cases of a cell with and without a buffer gas. We see that the absorption resonances appear only for large enough drive laser power Ω_d in the cell with a buffer gas. In the cell without any buffer gas the resonance remains dispersionlike ($\phi\approx\pi/2$) and vanishingly weak.

V. INFLUENCE OF THE BUFFER GAS ON FOUR-WAVE MIXING

So far we have completely ignored the presence of a Stokes field E_S in the medium. Many previous publications [36,50–52] have shown that dense coherent media contribute to significant enhancement of nonlinear processes. In our experiment the strong drive field applied to the $F=1$ level is scattered by the ground-state coherence, which leads to the appearance of narrow resonances in the Stokes field transmission with the width determined by the ground-state coherence relaxation rate. For near-resonant probe and drive fields ($\Delta\approx 0$) the Λ system formed by the Stokes and the

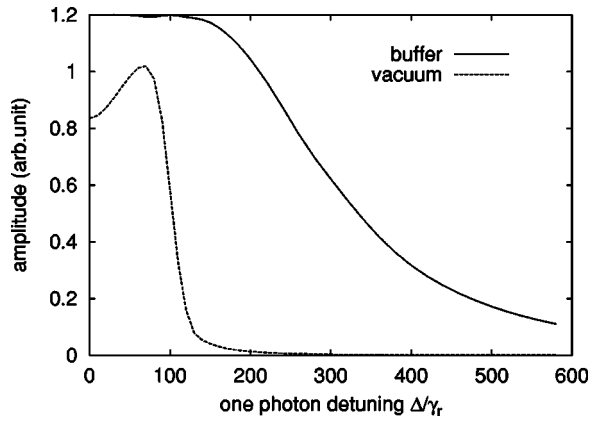

FIG. 10. Numerical calculation of the resonance strength (D) vs one-photon detuning for a probe field propagating in a medium with Ne buffer gas and with vacuum. One-photon detuning and resonance width are given in units of γ_r.

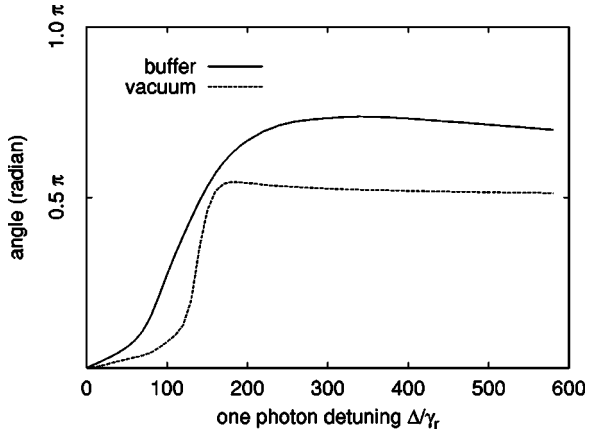

FIG. 11. Numerical calculation of angle (ϕ) vs one-photon detuning for a probe field propagating in a medium with Ne buffer gas and with vacuum. One-photon detuning and resonance width are given in units of γ_r.

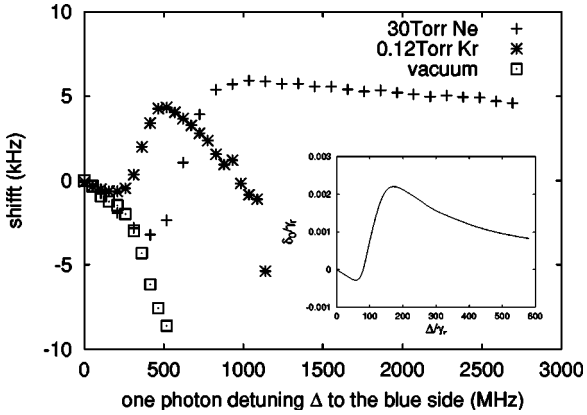

FIG. 12. Two-photon resonance shift (δ_0) as a function of one-photon detuning for the vacuum cell (squares), cell with 0.12 Torr of Kr (stars), and cell with 30 Torr of Ne (crosses). Inset: The result of the numerical simulation for the 30 Torr cell.

drive fields applied to the $F=1$ ground state level is far detuned [see Fig. 1(a)], and the effects of the associated ground-state coherence on the probe field are negligible. However, all four fields have to be taken into account in the case of large laser detuning, comparable with the ground-state hyperfine splitting.

The amplitude and the angle ϕ for the Stokes field transmission resonance in the cell with 30 Torr of Ne are shown in Fig. 13. Please note that for $\Delta=0$ we observe a dispersion-like line shape ($\phi\approx 0.5\pi$), which is different from the previously published experimental results for the Stokes field generation initiated by spontaneous photons [37]. As the laser detuning Δ increases the line shape of the Stokes field transmission changes, and the resonance is transformed into a symmetric transmission peak ($\phi\approx 0$).

VI. WIDTH OF THE PROBE AND STOKES RESONANCES

The measured widths of the two-photon resonance $\tilde{\gamma}$ as functions of the one-photon detuning Δ are shown in Fig. 14 for cells with different buffer gas pressure. Again we see the difference between cells with and without a buffer gas: in the

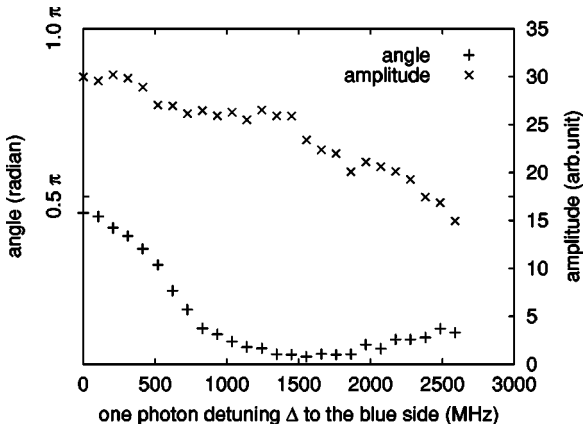

FIG. 13. Angle (ϕ) and amplitude (D) of the two-photon resonance for the generated Stokes field.

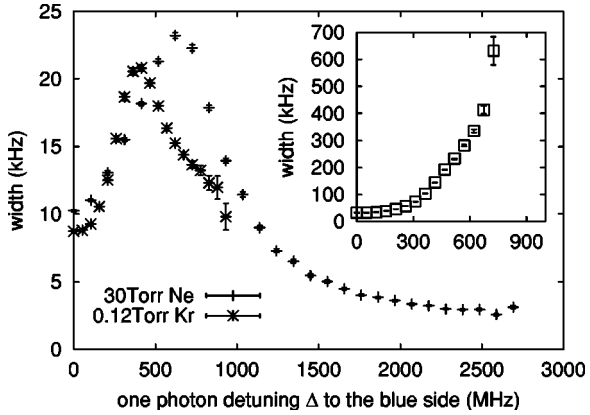

FIG. 14. Width of the two-photon resonance $\tilde{\gamma}$ as a function of one-photon detuning Δ for ^{87}Rb cell with 30 Torr of Ne (cross), 0.12 Torr of Kr ($\times$), and without buffer gas (squares, inset). The minimum width of the EIT resonance in the vacuum cell with no buffer gas is $\tilde{\gamma}(\Delta=0)=17$ kHz.

latter case the width of the EIT resonance increases significantly with one-photon detuning. However, for the buffered cells the resonance is broadened only near atomic resonance, but for larger detuning its width actually decreases with increasing Δ.

Figure 15 demonstrates that we may be able to observe the narrowing of resonances for large detuning even in a vacuum cell. However, according to Fig. 10 at the point when narrowing takes place ($\Delta/\gamma_r > 100$) the amplitude of the resonance is so small that it is extremely hard to detect in the experiment.

Narrow resonances with good signal-to-noise ratio are important for many applications. For example, narrow EIT resonances are used for precision metrology [16,53,54] and atomic clocks [55,56]. Our experiments demonstrate that the coherent absorption resonances, observed for the far-detuned Λ system, may have more attractive characteristics in terms of the resonance width and amplitude than the EIT resonances observed for zero detuning. For example, in the cell with 30 Torr of Ne the amplitude of the absorption resonance for $\Delta=1.2-2$ GHz is larger than that of the EIT reso-

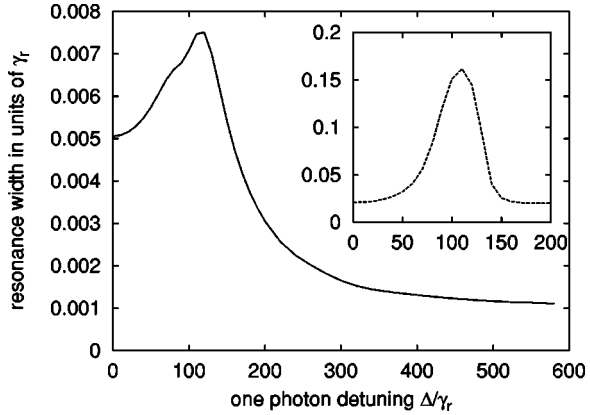

FIG. 15. Numerical calculation of resonance width ($2\tilde{\gamma}$) vs one-photon detuning for a probe field propagating in a medium with Ne buffer gas and with vacuum (inset).

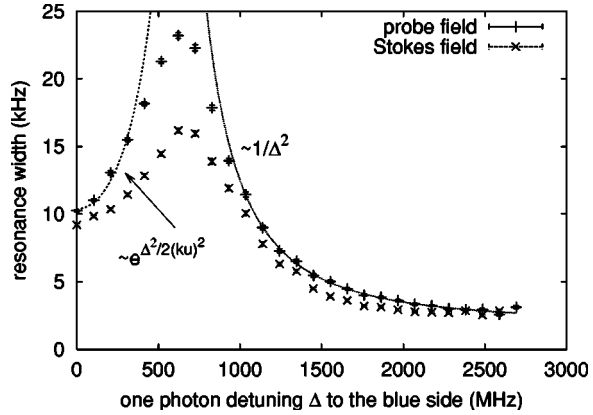

FIG. 16. Width of the two-photon resonance (γ) for the probe and generated Stokes field.

nance, while its width is narrower [for example, $\tilde{\gamma}(0)/\tilde{\gamma}(2\ \mathrm{GHz}) \approx 3.3$].

According to Eq. (17), in the strong laser field limit ($|\Omega_d|^2 \gg \gamma_{bc}\gamma$) the width of the EIT resonance for small Δ does not depend on the ground-state coherence decay rate and is determined by power broadening, $\tilde{\gamma} \approx |\Omega_d|^2/\gamma$, as in previous studies [38]. The resonance width decreases with one-photon detuning, and for $\Delta \gg \gamma$ it drops as $1/\Delta^2$. Ultimately, for $\Delta \gg |\Omega_d|\sqrt{\gamma/\gamma_{bc}}$, the width of the resonance is determined by the coherence decay rate γ_{bc}.

To describe the resonance width more carefully we again have to take into account the velocity distribution of Rb atoms in the cell. The variation of the laser field intensities as they propagate through the optically dense Rb vapor also becomes important; for example, the resonance width is reduced due to the density narrowing [57,58]. We note that the two effects are not very important for far-detuned optical fields ($\Delta \gg \gamma, ku$) since the absorption of the medium is small, and the parameters describing the resonance line shape do not change noticeably within the Doppler contour. Thus, for large detuning the dependence of the resonance width predicted by Eq. (17) is in good agreement with the experimental points, as shown in Fig. 16.

To describe how the resonance width changes for small Δ we should take both propagation and Doppler averaging into account. Since it is virtually impossible to do that exactly, we make a few simplifications that allow us to roughly predict the dependence of the resonance width on one-photon detuning. First, we assume that the main contribution to the observed resonance comes from the velocity subgroup for which $\Delta - kv \simeq 0$, i.e., the coupling fields are resonant with the atomic transitions. Then the main consequence of the laser detuning is the reduction of the number of atoms in this velocity group:

$$N(\Delta) \propto N e^{-\Delta^2/(ku)^2}. \tag{23}$$

Under these conditions the output intensity I_{out} is given by

$$I_{\mathrm{out}} \simeq I_{\mathrm{in}} e^{-\kappa L \gamma_{bc}/|\Omega_d|^2} e^{-\kappa L \gamma \delta^2/|\Omega_d|^4}. \tag{24}$$

In this expression the first term represents the residual absorption under EIT conditions, and the second one describes the shape of the peak as a function of two-photon detuning. It is easy to see that the width of the resonance in this case is inversely proportional to the atomic density [57]:

$$\tilde{\gamma}_D(N) \simeq \frac{|\Omega_d|^2}{\sqrt{\gamma\gamma_r}} \left(\frac{3}{8\pi} N \lambda^2 L \right)^{-1/2}. \tag{25}$$

Substituting the density of the resonant atoms given by Eq. (23) we obtain the resonance width:

$$\tilde{\gamma}_D(\Delta) \propto \frac{|\Omega_d|^2}{\sqrt{\gamma\gamma_r}} \frac{1}{\sqrt{NL}} e^{\Delta^2/2(ku)^2}. \tag{26}$$

Figure 16 shows that this formula works only for a small frequency region in the vicinity of one-photon resonance where the resonance is nearly symmetric and deviates for larger Δ, which is consistent with the assumptions we made.

The width of the Stokes field resonance is also shown in Fig. 16. It has approximately the same shape as the curve for the probe field, but it is worth mentioning that its width can be narrower than that of the probe field while having a similar resonance amplitude.

VII. ENHANCED ABSORPTION DUE TO ZEEMAN COHERENCE

Let us now consider another kind of coherence effect originating from coherent population trapping, namely, nonlinear magneto-optical polarization rotation. An extensive review of this effect is given in Ref. [59]. In this case, long-lived coherence is created among ground-state Zeeman sublevels by a single electromagnetic field (in general elliptically polarized but usually taken as linear in most experiments and analyses) where the Λ link(s) are formed by the two opposite circularly polarized components $E_{\pm}$ of the input field [Fig. 1(b)]. In this configuration the transmission is very sensitive to the applied magnetic field, which shifts sublevels with different magnetic quantum number m. An applied magnetic field B therefore creates a two-photon detuning δ proportional to the magnetic field: $\delta = 2\mu_B B/\hbar$, where μ_B is the Bohr magneton. In particular, the polarization of the incident laser field is changed dramatically as a result of the steep dispersion associated with CPT [60,61]. This effect, known as the nonlinear Faraday effect, or nonlinear magneto-optical polarization rotation, has been extensively studied over recent decades in atomic beams [62,63] and in glass cells with or without antirelaxation coating [60,61,64–70].

There are a number of publications that demonstrate strong influence of a buffer gas on the amplitude and line shape of polarization rotation and EIT resonances [71,72]. Here we show that the presence of a buffer gas also allows observation of narrow enhanced absorption peaks for buffer gas pressure higher than 3 Torr.

The transmission spectrum of ^{87}Rb $5S_{1/2}F=2 \rightarrow 5P_{1/2}$ $F'=1,2$ consists of two transitions, partially resolved within the Doppler contour as shown in Fig. 1(b). Zeeman coherence can be created on both transitions so that linear absorption is suppressed for a linearly polarized electromagnetic field even if the laser frequency differs somewhat from the exact atomic transition frequency. For example, if the laser is tuned

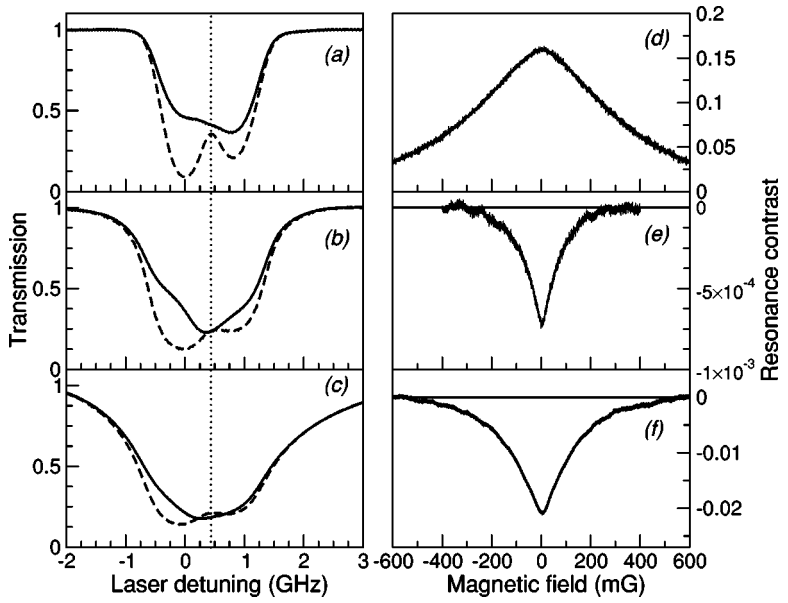

FIG. 17. Left column: Transmission through ^{87}Rb cells with (a) 1 Torr; (b) 3 Torr and (c) 10 Torr of Ne buffer gas as the laser frequency is swept across the $F=2\rightarrow F'$ transitions. Solid line: Transmission at zero magnetic field. In this case the ground-state coherence is unperturbed and we denote the transmission as T_{coh}. Dashed line: Transmission at large magnetic field ($\delta \gg \gamma_0$). In this case the coherence is destroyed, and we denote the transmission as T_{lin}. Right column: The peak contrast in transmission as a function of magnetic field (two-photon detuning) for fixed laser frequency (shown as a dotted line on the previous graphs) for the same cells. The normalization of the output signal is $C=(T_{coh}-T_{lin})/T_{coh}$. Thus $C>0$ is a manifestation of EIT shown in part (d), and $C<0$ indicates enhanced absorption as seen in (e) and (f). Because of the difference in geometrical size of the cells, the atomic density is adjusted for each case so that $T_{lin}\sim 20\%$. Laser power is 2 mW.

exactly between the two transitions ($\Delta=406$ MHz), the transmission is still enhanced by 40%.

This is true, however, only if there is no buffer gas present in the cell. The transmission spectra for different pressures of Ne buffer gas are shown in Figs. 17(a)–17(c). One can easily see that the effect of EIT deteriorates at higher buffer gas pressures. Moreover, the enhanced absorption appears for the frequency region between the two transitions. When the magnetic field is varied the width of the observed resonances is similar to that of the EIT peak as shown in Figs. 17(d)–17(f), which indicates that this effect is due to the ground-state coherence. Similar resonances have been observed in cells with antirelaxation wall coating [74].

Here we should emphasize that the reason for the enhanced absorption resonances described in this section is quite different from the effects described in the previous sections, despite their similarities (both effects are observed only in buffered Rb cells and for nonzero one-photon detunings). In the case of Zeeman coherence, the nonlinear enhanced absorption may be explained by the interplay of the matrix elements of the transitions involved in the Λ links. As the laser frequency changes, dark states can be created for both $F=2\rightarrow F'=1$ and $F=2\rightarrow F'=2$ transitions. However, because of the difference in relative sign in the transition matrix elements [48], these dark states are orthogonal:

$$|D\rangle_{2\rightarrow 1}=\frac{1}{\sqrt{2}}(|m=1\rangle+|m=-1\rangle), \tag{27}$$

$$|D\rangle_{2\rightarrow 2}=\frac{1}{\sqrt{2}}(|m=1\rangle-|m=-1\rangle). \tag{28}$$

Strictly speaking, because of this difference, perfect CPT is not possible in this double-Λ system. However, the natural width of both transitions ($\gamma_r\simeq 3$ MHz) is much smaller than their hyperfine splitting, and for the laser resonant with one transition, the disturbance introduced by the other transition may be neglected. For a cell without buffer gas or antirelaxation coating, atoms do not change their velocity while moving through the laser beam, and interact with the same atomic transition. Therefore we observe two Gaussian-shaped transmission peaks as the laser frequency is swept across the $F=2\rightarrow F'$ transitions.

In the presence of a buffer gas the situation is different. Since the hyperfine structure of the excited level is not completely resolved under Doppler broadening, there is a finite probability that an atom, optically pumped into the dark state on one transition, may later change its velocity and become resonant with the other transition. Because of the sign difference, the previously prepared dark state becomes a bright state for that transition, and the atom absorbs light more readily than the one without coherence. Thus, for the symmetric scheme shown in Fig. 1(b), we would expect complete destruction of coherence for the laser tuned exactly between two atomic transitions, so that the probabilities of an atom interacting with either of them are equal. In reality, however, the $F=2\rightarrow F'=1$ transition is stronger then the $F=2\rightarrow F'=2$ transition, and this imbalance results in en-

hanced absorption for a small region of laser frequencies.

VIII. SUMMARY

We have demonstrated significant changes of the EIT resonance in warm Rb vapor with a buffer gas. We showed that the resonance line shape changes from a symmetric transparency peak to a dispersionlike signal and then to a nearly symmetric absorption peak as one-photon detuning of the laser fields from atomic transition increases. We also found that for large enough detuning the resonance width was limited by the ground level coherence decay rate (γ_{bc}), and there is a region of laser frequencies with higher resonance contrast than for zero one-photon detuning, while the width of the resonance is narrower. Observation of this absorptionlike resonance is power dependent and takes place only for high enough drive power. We have also developed a simple theory and performed numerical stimulations that qualitatively describe the observations, and we have accounted for the origin of the discrepancies between those and the experimental data. We compared the behavior of the probe and Stokes fields for large one-photon detuning, and showed that the resonance width of these two fields behaves similarly, while the shapes of the resonances are different.

We have also shown that an induced absorption resonance appears with one-photon detuning in the Hanle configuration, although its origin differs from that in the bichromatic case. In the Hanle configuration, the enhanced absorption results from the destructive interference between the dark states created via different excited states in the presence of velocity changing collisions.

The effects reported here differ from previously observed electromagnetically induced absorption resonances and the absorption Hanle effect. Both of those cases have strict requirements on selection rules that are not required or met for our observations.

ACKNOWLEDGMENTS

We thank V. A. Sautenkov, D. Budker, A. B. Matsko, A. Zhang, and M. O. Scully for useful and stimulating discussions, and M. Klein for careful reading of the manuscript. Financial support is provided by the Office of Naval Research.

[1] E. Arimondo and G. Orriols, Lett. Nuovo Cimento Soc. Ital. Fis. **17**, 333 (1976).
[2] B. D. Agapyev, M. B. Gornyi, B. G. Matisov, and Y. V. Rozhdestvenskii, Usp. Fiz. Nauk **163**, 1 (1993).
[3] E. Arimondo, Prog. Opt. **35**, 259 (1996).
[4] M. O. Scully and M. S. Zubairy, *Quantum Optics* (Cambridge University Press, Cambridge, U.K., 1997).
[5] S. E. Harris, Phys. Today **50**(7), 36 (1997).
[6] J. P. Marangos, J. Mod. Opt. **45**, 471 (1998).
[7] S. E. Harris, J. E. Field, and A. Kasapi, Phys. Rev. A **46**, R29 (1992).
[8] O. Schmidt, R. Wynands, Z. Hussein, and D. Meschede, Phys. Rev. A **53**, R27 (1996).
[9] F. Renzoni and E. Arimondo, Opt. Commun. **178**, 345 (2000).
[10] E. Arimondo, Phys. Rev. A **54**, 2216 (1996).
[11] M. Graf, E. Arimondo, E. S. Fry, D. E. Nikonov, G. G. Padmabandu, M. O. Scully, and S. Y. Zhu, Phys. Rev. A **51**, 4030 (1995).
[12] R. Bernheim, *Optical Pumping* (W. A. Benjamin, New York, 1965).
[13] J. Vanier, A. Godone, and F. Levi, Phys. Rev. A **58**, 2345 (1998).
[14] W. Happer, Rev. Mod. Phys. **44**, 169 (1972).
[15] S. Brandt, A. Nagel, R. Wynands, and D. Meschede, Phys. Rev. A **56**, R1063 (1997).
[16] R. Wynands and A. Nagel, Appl. Phys. B: Lasers Opt. **68**, 1 (1998).
[17] M. Erhard, S. Nußmann, and H. Helm, Phys. Rev. A **62**, 061802(R) (2000).
[18] M. Erhard and H. Helm, Phys. Rev. A **63**, 043813 (2001).
[19] E. E. Mikhailov, V. A. Sautenkov, Y. V. Rostovtsev, and G. R. Welch, J. Opt. Soc. Am. B **21**, 425 (2004).
[20] E. E. Mikhailov, V. A. Sautenkov, I. Novikova, and G. R. Welch, Phys. Rev. A **69**, 063808 (2004).
[21] C. Affolderbach, S. Knappe, R. Wynands, A. V. Taichenachev, and V. I. Yudin, Phys. Rev. A **65**, 043810 (2002).
[22] A. M. Akulshin, S. Barreiro, and A. Lezama, Phys. Rev. A **57**, 2996 (1998).
[23] A. Lezama, S. Barreiro, and A. M. Akulshin, Phys. Rev. A **59**, 4732 (1999).
[24] A. Lipsich, S. Barreiro, A. M. Akulshin, and A. Lezama, Phys. Rev. A **61**, 053803 (2000).
[25] A. V. Taichenachev, A. M. Tumaikin, and V. I. Yudin, JETP Lett. **69**, 819 (1999).
[26] A. V. Taichenachev, A. M. Tumaikin, and V. I. Yudin, Phys. Rev. A **61**, 011802 (2000).
[27] M. Kwon, K. Kim, H. S. Moon, H. D. Park, and J. B. Kim, J. Phys. B **34**, 2951 (2001).
[28] C. Y. Ye, Y. V. Rostovtsev, A. S. Zibrov, and Y. M. Golubev, Opt. Commun. **207**, 227 (2002).
[29] Y. Dancheva, G. Alzetta, S. Cartaleva, M. Taslakov, and C. Andreeva, Opt. Commun. **178**, 103 (2000).
[30] G. Alzetta, S. Cartaleva, Y. Dancheva, C. Andreeva, S. Gozzini, L. Botti, and A. Rossi, J. Opt. B: Quantum Semiclassical Opt. **3**, 181 (2001).
[31] F. Renzoni, C. Zimmermann, P. Verkerk, and E. Arimondo, J. Opt. B: Quantum Semiclassical Opt. **3**, S7 (2001).
[32] F. Renzoni, S. Cartaleva, G. Alzetta, and E. Arimondo, Phys. Rev. A **63**, 065401 (2001).
[33] C. Andreeva, S. Cartaleva, Y. Dancheva, V. Biancalana, A. Burchianti, C. Marinelli, E. Mariotti, L. Moi, and K. Nasyrov, Phys. Rev. A **66**, 012502 (2002).
[34] H. Failache, P. Valente, G. Ban, V. Lorent, and A. Lezama, Phys. Rev. A **67**, 043810 (2003).
[35] G. S. Agarwal, Adv. At., Mol., Opt. Phys. **29**, 113 (1991).
[36] M. M. Kash, V. A. Sautenkov, A. S. Zibrov, L. Hollberg, G. R.

Welch, M. D. Lukin, Y. Rostovtsev, E. S. Fry, and M. O. Scully, Phys. Rev. Lett. **82**, 5229 (1999).
[37] E. E. Mikhailov, Y. Rostovtsev, and G. R. Welch, J. Mod. Opt. **49**, 2535 (2002).
[38] A. Javan, O. Kocharovskaya, H. Lee, and M. O. Scully, Phys. Rev. A **66**, 013805 (2002).
[39] Y. Rostovtsev, I. Protsenko, H. Lee, and A. Javan, J. Mod. Opt. **49**, 2501 (2002).
[40] E. Kuznetsova, O. Kocharovskaya, P. Hemmer, and M. O. Scully, Phys. Rev. A **66**, 063802 (2002).
[41] H. Lee, Y. Rostovtsev, C. J. Bednar, and A. Javan, Appl. Phys. B: Lasers Opt. **76**, 33 (2003).
[42] F. Levi, A. Godone, J. V. S. Micalizio, and G. Modugno, Eur. Phys. J. D **12**, 53 (2000).
[43] S. Knappe, M. Stahler, C. Affolderbach, A. Taichenachev, V. Yudin, and R. Wynands, Appl. Phys. B: Lasers Opt. **76**, 57 (2003).
[44] A. V. Taichenachev, V. I. Yudin, R. Wynands, M. Stähler, J. Kitching, and L. Hollberg, Phys. Rev. A **67**, 033810 (2003).
[45] Y. Li and M. Xiao, Phys. Rev. A **51**, 4959 (1995).
[46] B. Lounis and C. Cohen-Tannoudji, J. Phys. II **2**, 579 (1992).
[47] C. Ottinger, R. Scheps, G. W. York, and A. Gallagher, Phys. Rev. A **11**, 1815 (1975).
[48] J. Vanier and C. Audoin, *The Quantum Physics of Atomic Frequency Standards*, Vol. 1 (Adam Hilger, Philadelphia, 1989).
[49] W. Happer, Rev. Mod. Phys. **44**, 169 (1972).
[50] M. D. Lukin, M. Fleischhauer, A. S. Zibrov, H. G. Robinson, V. L. Velichansky, L. Hollberg, and M. O. Scully, Phys. Rev. Lett. **79**, 2959 (1997).
[51] S. E. Harris and L. V. Hau, Phys. Rev. Lett. **82**, 4611 (1999).
[52] M. T. Johnsson and M. Fleischhauer, Phys. Rev. A **66**, 043808 (2002).
[53] C. Affolderbach, M. Stahler, S. Knappe, and R. Wynands, Appl. Phys. B: Lasers Opt. **75**, 605 (2002).
[54] D. Budker, D. F. Kimball, S. M. Rochester, V. V. Yashchuk, and M. Zolotorev, Phys. Rev. A **62**, 043403 (2000).
[55] J. Kitching, S. Knappe, and L. Hollberg, Appl. Phys. Lett. **81**, 553 (2002).
[56] M. Merimaa, T. Lindvall, I. Tittonen, and E. Ikonen, J. Opt. Soc. Am. B **20**, 273 (2003).
[57] M. D. Lukin, M. Fleischhauer, A. S. Zibrov, H. G. Robinson, V. L. Velichansky, L. Hollberg, and M. O. Scully, Phys. Rev. Lett. **79**, 2959 (1997).
[58] V. Sautenkov, M. Kash, V. Velichansky, and G. Welch, Laser Phys. **9**, 889 (1999).
[59] D. Budker, W. Gawlik, D. Kimball, S. Rochester, V. Yashchuk, and A. Weis, Rev. Mod. Phys. **74**, 1153 (2002).
[60] V. A. Sautenkov, M. D. Lukin, C. J. Bednar, I. Novikova, E. Mikhailov, M. Fleischhauer, V. L. Velichansky, G. R. Welch, and M. O. Scully, Phys. Rev. A **62**, 023810 (2000).
[61] I. Novikova, A. B. Matsko, and G. R. Welch, Opt. Lett. **26**, 1016 (2001).
[62] G. Théobald, N. Dimarcq, V. Giordano, and P. Cérez, Opt. Commun. **71**, 256 (1989).
[63] B. Schuh, S. I. Kanorsky, A. Weis, and T. W. Hansch, Opt. Commun. **100**, 451 (1993).
[64] K. H. Drake, W. Lange, and J. Mlynek, Opt. Commun. **66**, 315 (1988).
[65] L. M. Barkov, D. A. Melik-Pashaev, and M. S. Zolotorev, Opt. Commun. **70**, 467 (1989).
[66] P. E. G. Baird, M. Irie, and T. D. Wolfenden, J. Phys. B **22**, 1733 (1989).
[67] X. Chen, V. L. Telegdi, and A. Weis, Opt. Commun. **78**, 337 (1990).
[68] S. I. Kanorsky, A. Weis, and J. Skalla, Appl. Phys. B: Lasers Opt. **60**, S165 (1995).
[69] D. Budker, V. Yashchuk, and M. Zolotorev, Phys. Rev. Lett. **81**, 5788 (1998).
[70] D. Budker, D. J. Orlando, and V. Yashchuk, Am. J. Phys. **67**, 584 (1999).
[71] A. S. Zibrov, I. Novikova, and A. B. Matsko, Opt. Lett. **26**, 1311 (2001).
[72] I. Novikova, A. B. Matsko, and G. R. Welch, Appl. Phys. Lett. **81**, 193 (2002).
[73] U. D. Rapol, A. Wasan, and V. Natarajan, Phys. Rev. A **67**, 053802 (2003).
[74] D. Budker (private communication).